

**NIST Technical Note  
NIST TN 2227**

**Data assimilation in 2D nonlinear  
advection diffusion equations, using  
an explicit  $O(\Delta t)^2$  stabilized leapfrog  
scheme run backward in time**

Alfred S. Carasso

This publication is available free of charge from:  
<https://doi.org/10.6028/NIST.TN.2227>

**NIST Technical Note  
NIST TN 2227**

**Data assimilation in 2D nonlinear  
advection diffusion equations, using  
an explicit  $O(\Delta t)^2$  stabilized leapfrog  
scheme run backward in time**

Alfred S. Carasso  
*Applied and Computational Mathematics Division  
Information Technology Laboratory*

This publication is available free of charge from:  
<https://doi.org/10.6028/NIST.TN.2227>

July 2022



U.S. Department of Commerce  
*Gina M. Raimondo, Secretary*

National Institute of Standards and Technology  
*Laurie E. Locascio, NIST Director and Under Secretary of Commerce for Standards and Technology*

Certain commercial entities, equipment, or materials may be identified in this document in order to describe an experimental procedure or concept adequately. Such identification is not intended to imply recommendation or endorsement by the National Institute of Standards and Technology, nor is it intended to imply that the entities, materials, or equipment are necessarily the best available for the purpose.

### **NIST Technical Series Policies**

[Copyright, Fair Use, and Licensing Statements](#)

[NIST Technical Series Publication Identifier Syntax](#)

### **Publication History**

Approved by the NIST Editorial Review Board on 2022-07-05

### **How to cite this NIST Technical Series Publication:**

Alfred S. Carasso (2022) Data assimilation in 2D nonlinear advection diffusion equations, using an explicit  $O(\Delta t)^2$  stabilized leapfrog scheme run backward in time. (National Institute of Standards and Technology, Gaithersburg, MD), NIST TN 2227. <https://doi.org/10.6028/NIST.TN.2227>

## Abstract

With an artificial example of a 2D nonlinear advection diffusion equation on the unit square in  $R^2$ , this paper considers the data assimilation problem of finding initial values  $u(x, y, 0)$ , that can evolve into a close approximation to a desired target result  $u^*(x, y, T)$ , at some realistic  $T > 0$ . Highly non smooth target data are considered, that may not correspond to actual solutions at time  $T$ , and it may not be possible to find such initial values. The aim is to illustrate the inherent difficulties of the ill-posed data assimilation problem, while demonstrating the use of a powerful computational tool. An explicit,  $O(\Delta t)^2$  accurate, stable marching finite difference scheme, that can be run forward or backward in time, is used to find candidate initial values corresponding to the target data. These initial values are then marched forward, and compared to the target data. Instructive successful and unsuccessful examples are presented, using non smooth target data corresponding to 8 bit,  $512 \times 512$  pixel gray-scale images of recognizable objects. The above explicit scheme may also be helpful in conjunction with more elaborate and computationally intensive assimilation methods, by providing a preliminary assessment of target feasibility, as well as possibly useful initial results.

## Keywords

2D time-reversed advection diffusion equations; numerical experiments; non smooth data assimilation; stabilized leapfrog scheme.

## Table of Contents

1. Introduction	1
2. Use of Computational Examples Based on Sharp Image Data	2
3. Stabilized Leapfrog Scheme in the Unit Square	3
4. Fourier Stability Analysis in Linearized Problem	5
5. Leapfrog Nonlinear Computational Instability and the RAW Filter	11
6. 2D Nonlinear Computational Experiments	12
7. Concluding Remarks	14
References	20

## List of Tables

Table 1.	9
Table 2.	15
Table 3.	16
Table 4.	17
Table 5.	18
Table 6.	19

## List of Figures

Fig. 2.	Target data at time $T$ , in leftmost column, are marched backward in time to obtain candidate initial data in middle column. When marched forward to time $T$ , middle column data evolve into rightmost column. Quantitative error estimates are provided in Table 2.	15
Fig. 3.	Target data at time $T$ , in leftmost column, are marched backward in time to obtain candidate initial data in middle column. When marched forward to time $T$ , middle column data evolve into rightmost column. Quantitative error estimates are provided in Table 3.	16
Fig. 4.	Target data at time $T$ , in leftmost column, are marched backward in time to obtain candidate initial data in middle column. When marched forward to time $T$ , middle column data evolve into rightmost column. Quantitative error estimates are provided in Table 4.	17
Fig. 5.	Target data at time $T$ , in leftmost column, are marched backward in time to obtain candidate initial data in middle column. When marched forward to time $T$ , middle column data evolve into rightmost column. Quantitative error estimates are provided in Table 5.	18
Fig. 6.	Target data at time $T$ , in leftmost column, are marched backward in time to obtain candidate initial data in middle column. When marched forward to time $T$ , middle column data evolve into rightmost column. Quantitative error estimates are provided in Table 6.	19

## 1. Introduction

This paper uses an artificial example of a 2D nonlinear advection diffusion equation, together with highly non-smooth target data associated with gray scale images of recognizable objects, to illustrate the inherent difficulties of *data assimilation* in such equations. In addition, the usefulness of a direct non iterative computational tool, in the form of an explicit,  $O(\Delta t)^2$  accurate, stable marching finite difference scheme, is demonstrated. That scheme can be run forward or backward in time.

As is evident from Refs. [1–12] and the references therein, advection diffusion equations play an important role in environmental and geophysical sciences, and there is increasing interest in backward in time data assimilation computations. However, in many dissipative evolution equations, such ill-posed inverse computations may fail to produce useful information, even with sophisticated regularization. This might be anticipated on the basis of the rigorous uncertainty estimates discussed in Refs. [13–20]. As was stressed in the  $O(\Delta t)$  approach to the 2D Burgers equation developed in Ref. [12], data assimilation is fundamentally different from the more familiar backward recovery problem discussed in Refs. [21, 22], where initial values are sought from noisy data at time  $T > 0$ , approximating an *actual solution* to within a *known small*  $\delta > 0$  in the  $\mathcal{L}^2$  norm. In data assimilation, the desired target data at time  $T > 0$  may differ from an actual solution by an *unknown large*  $\delta > 0$  in the  $\mathcal{L}^2$  norm.

The present paper seeks to draw attention to the *limited feasibility* of data assimilation, by presenting instructive examples of successful as well as unsuccessful assimilation, and by exploring the important role played by the coefficient values in the given evolution equation, as well as the value of  $T > 0$ . Significantly, the  $O(\Delta t)^2$  stabilized explicit leapfrog scheme discussed in Refs. [21, 22] can be used effectively for that purpose.

In the unit square  $\Omega \subset R^2$ , with homogeneous boundary conditions on  $\partial\Omega$ , and positive coefficients  $\alpha(u)$ ,  $q(x,y)$ , we study 2D nonlinear parabolic equations of the form

$$u_t = \alpha(u)\nabla \cdot \{q(x,y)\nabla u\} + \beta(u)u_x + \gamma(u)u_y. \quad (1)$$

The following *data assimilation/inverse design problem* associated with Eq. (1) is considered: With appropriate  $T > 0$ , find initial values  $u(x,y,0)$  that can evolve into a close approximation to a desired target result  $u^*(x,y,T)$ , at time  $T$ . Here, highly non smooth target data are considered that *may not correspond to actual solutions* of Eq. (1) at time  $T$ , and it *may not be possible* to find such initial values.

The stabilized explicit leapfrog scheme discussed in Refs. [21, 22], is a direct, non iterative, stepwise computational method, that can be run forward or backward in time. Using this tool, examples are presented where useful initial values can be found that evolve into good approximations to the target data  $u^*(x,y,T)$ , with modestly small  $\mathcal{L}^1$  relative errors. Such examples become even more successful with smaller values of  $T$ , but less successful with larger  $T$ . However, there are also examples where the resulting  $\mathcal{L}^1$  relative errors at time

$T$  are not small, although the computed solutions exhibit important characteristic features associated with the desired targets  $u^*(x, y, T)$ . Here, the fast and accurate explicit leapfrog scheme allows easy interactive exploration of whether closer agreement might result with reduced coefficients  $\alpha$ ,  $q$ ,  $\beta$ ,  $\gamma$ , in Eq. (1). This is of interest in many applications where the evolution equation governing the process is only tentatively known, and appropriate readjustment of coefficients is anticipated. Finally, with a given  $T > 0$ , and a given evolution equation in Eq. (1), there are examples of target data  $u^*(x, y, T)$ , for which useful initial values *cannot* be found using this computational tool.

The above direct approach may also be helpful if used in conjunction with more elaborate data assimilation procedures, based on neural networks and machine learning, by providing a preliminary assessment of the feasibility of the desired target data  $u^*(x, y, T)$ , with the given evolution equation and value of  $T > 0$ . Successful leapfrog results may also provide valuable initial guesses that might be improved by subsequent processing with other methods.

**IMAGES ARE DEFINED BY HIGHLY NON SMOOTH INTENSITY DATA THAT CHALLENGE ILL-POSED RECOVERY METHODS**

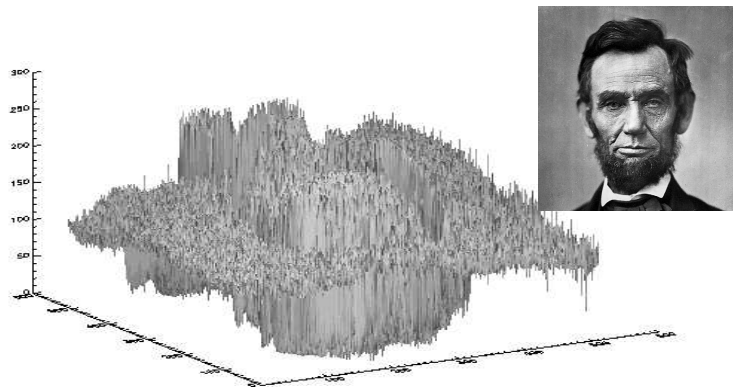


**Fig. 1.** Plot of intensity values  $f(x, y)$  versus  $(x, y)$ , in  $512 \times 512$  pixel Abe Lincoln image. Intensity values range from 0 to 255, and result in a highly non smooth surface. Similar characteristics are found in numerous images of easily recognizable objects. Such images are not of bounded variation [23], present significant computational challenges, and provide instructive examples in data assimilation experiments.

## 2. Use of Computational Examples Based on Sharp Image Data

As in Refs. [12, 21, 22], numerical experiments will be presented involving 8 bit,  $512 \times 512$  pixel gray-scale images. As illustrated in Fig. 1, many images of easily recognizable objects

are defined by non smooth intensity data  $f(x,y)$ , that would be quite difficult to synthesize mathematically. These images are not of bounded variation. Rather, as shown in Ref. [23], with  $0 < \alpha < 0.7$ , and  $|h| = (h_1^2 + h_2^2)^{1/2}$ , they belong to the Lipschitz class  $\Lambda(\alpha, 1, \infty)$ , of functions  $f(x,y)$  satisfying

$$\int_{\mathbb{R}^2} |f(x+h_1, y+h_2) - f(x,y)| dx dy \leq Const. |h|^\alpha, \quad |h| \downarrow 0, \quad (2)$$

while images of bounded variation require  $\alpha = 1$ . Such non smooth images pose significant challenges in ill-posed reconstruction, and they constitute an invaluable tool for *exploring* the possibility of computing a wide variety of dissipative evolution equations backward in time. In the present application, in addition to quantitative metrics of success or failure applied to the underlying data, such as relative errors in various  $\mathcal{L}^p$  norms, and peak signal to noise ratios (PSNR), the ability to view the assimilated data as an image, is quite helpful.

The approach to be used is based on marching backward in time from the given target data at time  $T$ , using an  $O(\Delta t)^2$  explicit finite difference scheme. As is well-known [24, p. 59], for ill-posed initial value problems, every consistent stepwise marching scheme, whether explicit or implicit, is necessarily *unconditionally unstable*. However, as shown in Refs. [12, 21, 22], it is possible to stabilize explicit marching schemes by applying an appropriate compensating smoothing operator at each time step to quench the instability. This renders the scheme unconditionally *stable*, but slightly inconsistent. In backward reconstructions from relatively smooth data known to closely approximate the exact solutions at time  $T$ , the cumulative error caused by such smoothing is sufficiently small to allow for useful results. Unexpectedly, such stabilized schemes may sometimes be useful in data assimilation with non smooth targets at time  $T$ , by using more aggressive smoothing at each time step.

Below, we review error bounds obtained in the recently developed schemes in Refs. [21, 22]. A simplified linear analysis in Sections 4 and 5 below, leads to the error estimates in Theorems 1 and 2 at the end of Section 4, together with the important Remark 2. These results examine the feasibility of data assimilation, and set the stage for the nonlinear computational experiments discussed in Section 6.

### 3. Stabilized Leapfrog Scheme in the Unit Square

Let  $\Omega$  be the unit square in  $\mathbb{R}^2$  with boundary  $\partial\Omega$ . Let  $\langle \cdot, \cdot \rangle$  and  $\| \cdot \|_2$ , respectively denote the scalar product and norm on  $\mathcal{L}^2(\Omega)$ . With  $(x,y,t) \in \Omega \times (0,T]$ , positive  $\alpha(u)$  and  $q(x,y)$ , initial values  $u(x,y,0) = u_0(x,y)$ , and homogeneous boundary conditions on  $\partial\Omega \times [0,T]$ , we now consider the evolution equation in Eq. (1),

$$u_t = L^\dagger u \equiv \alpha(u) \nabla \cdot \{q(x,y) \nabla u\} + \beta(u) u_x + \gamma(u) u_y. \quad (3)$$

The well-posed forward initial value problem in Eq. (3) becomes ill-posed if the time direction is reversed, and one wishes to recover  $u(x,y,0)$  given desired target data  $u^*(x,y,T)$ .

We contemplate both forward and time-reversed computations by allowing for possible *negative time steps*  $\Delta t$  in the leapfrog time-marching finite difference scheme to be described below. With a given positive integer  $N$ , let  $|\Delta t| = T/(N + 1)$  be the time step magnitude, and let  $\tilde{u}^n(x, y) \equiv \tilde{u}(x, y, n\Delta t)$ ,  $n = 1, \dots, N + 1$ , denote the intended approximation to  $u(x, y, n\Delta t)$ . It is helpful to consider Fourier series expansions for  $\tilde{u}^n(x, y)$ , on the unit square  $\Omega$ ,

$$\tilde{u}^n(x, y) = \sum_{j, k=-\infty}^{\infty} \tilde{u}_{j, k}^n \exp\{2\pi i(jx + ky)\}, \quad (4)$$

with Fourier coefficients  $\{\tilde{u}_{j, k}^n\}$  given by

$$\tilde{u}_{j, k}^n = \int_{\Omega} \tilde{u}^n(x, y) \exp\{-2\pi i(jx + ky)\} dx dy, \quad (5)$$

With given fixed  $\omega > 0$  and  $p > 1$ , define  $\lambda_{j, k}$ ,  $\sigma_{j, k}$ , as follows

$$\lambda_{j, k} = 4\pi^2(j^2 + k^2), \quad \sigma_{j, k} = \exp\{-\omega|\Delta t|\lambda_{j, k}^p\}. \quad (6)$$

For any  $f(x, y) \in \mathcal{L}^2(\Omega)$ , let  $\{f_{j, k}\}$  be its Fourier coefficients as in Eq (5). Using Eq. (6), define the linear operators  $P$  and  $S$  as follows

$$\begin{aligned} Pf &= \sum_{j, k=-\infty}^{\infty} \lambda_{j, k}^p f_{j, k} \exp\{2\pi i(jx + ky)\}, & \forall f \in \mathcal{L}^2(\Omega), \\ Sf &= \sum_{j, k=-\infty}^{\infty} \sigma_{j, k} f_{j, k} \exp\{2\pi i(jx + ky)\}, & \forall f \in \mathcal{L}^2(\Omega). \end{aligned} \quad (7)$$

As in Refs. [12, 21, 22], the operator  $S$  will be used as a stabilizing smoothing operator at each time step. With the nonlinear operator  $L^\dagger$  as in Eq (3), let

$$L^\dagger \tilde{u}^n \equiv \alpha(\tilde{u}^n) \nabla \cdot \{q(x, y) \nabla \tilde{u}^n\} + \beta(x, y, \tilde{u}^n) \tilde{u}_x^n + \gamma(x, y, \tilde{u}^n) \tilde{u}_y^n. \quad (8)$$

Consider the following stabilized leapfrog time-marching difference scheme for the system in Eq (3), in which only the time variable is discretized, while the space variables remain continuous,

$$\begin{aligned} \tilde{u}^{n+1} &= S\tilde{u}^{n-1} + 2\Delta t SL^\dagger \tilde{u}^n, & n = 1, 2, \dots, N, \\ \tilde{u}^0(x, y) &= u_0(x, y), & \tilde{u}^1(x, y) = u_0(x, y) + \Delta t L^\dagger u_0. \end{aligned} \quad (9)$$

The above semi-discrete problem is highly nonlinear. The analysis presented in Sections 4 and 5 below, although limited to a related simplified linear problem, is relevant to the above semi-discrete problem. In Section 6, where actual numerical computations are discussed, a uniform grid is imposed on  $\Omega$ , the space variables are discretized using centered differencing, and FFT algorithms are used to synthesize the smoothing operator  $S$ .

#### 4. Fourier Stability Analysis in Linearized Problem

Useful insight into the behavior of the nonlinear scheme in Eq. (9) involving  $L^\dagger$ , can be gained by analyzing a related problem with constant coefficients, involving a linear operator  $L$ . With constants  $a, b, c$ , such that  $a, |b|, |c| > 0$ , consider the initial value problem on the unit square  $\Omega$ ,

$$\begin{aligned} u_t &= Lu \equiv a\Delta u + bu_x + cu_y, \quad 0 < t \leq T, \\ u(x, y, 0) &= u_0(x, y), \end{aligned} \quad (10)$$

together with homogeneous boundary conditions on  $\partial\Omega$ . Let  $|\Delta t| = T/(N+1)$ . With  $u(x, y, t)$  the unique solution in Eq. (10), let

$$\theta^1 = u(x, y, 0), \quad u^n(x, y) = u(x, y, n\Delta t), \quad n \geq 1. \quad (11)$$

Then, the exact solution  $u^n$  satisfies the following leapfrog system

$$\theta^{n+1} = u^n, \quad u^{n+1} = \theta^n + 2\Delta t Lu^n + \tau^n, \quad n = 1, 2, \dots, N, \quad (12)$$

where, for  $n = 1, 2, \dots, N$ , the truncation error term  $\tau^n$  is given by

$$\tau^n = \{(\Delta t)^3/6\} \{u_{ttt}(x, y, s)\}, \quad n|\Delta t| < |s| < (n+1)|\Delta t|. \quad (13)$$

Define the following two component vectors and matrix  $G$

$$V^n = [\theta^n, u^n]^T, \quad \Phi_\tau^n = [0, \tau^n]^T, \quad (14)$$

$$G = \begin{bmatrix} 0 & I \\ I & 2\Delta t L \end{bmatrix}. \quad (15)$$

One may then rewrite Eq. (12) as

$$V^{n+1} = GV^n + \Phi_\tau^n, \quad n = 1, 2, \dots, N. \quad (16)$$

Define  $\mathcal{L}^2(\Omega)$  norms for two component vectors  $W = [w^1 \ w^2]^T$ , and  $2 \times 2$  matrices  $H$ , as follows

$$\|W\|_2^2 = (\|w^1\|_2^2 + \|w^2\|_2^2), \quad \|H\|_2 = \sup_{\|W\|_2 \neq 0} \{\|HW\|_2 / \|W\|_2\}. \quad (17)$$

Also, for functions  $h(x, y, t)$  on  $\Omega \times [0, T]$ , define the norm  $\|h\|_{2, \infty}$  as follows

$$\|h\|_{2, \infty} \equiv \sup_{0 \leq t \leq T} \{\|h(\cdot, t)\|_2\}. \quad (18)$$

One may also write the stabilized leapfrog scheme for computing Eq. (10) in matrix-vector notation. Let

$$\tilde{\theta}^1(x, y) = u_0(x, y), \quad \tilde{u}^1(x, y) = u_0(x, y) + \Delta t Lu_0. \quad (19)$$

Then,

$$u(x, y, \Delta t) = \tilde{u}^1(x, y) + \tau^0, \quad (20)$$

$$\tau^0 = \{(\Delta t)^2/2\} \{u_{tt}(x, y, r)\}, \quad 0 < |r| < |\Delta t|.$$

With  $\tilde{V}^n = [\tilde{\theta}^n, \tilde{u}^n]^T$ , the operator  $S$  as in Eq. (7), and matrix  $\Lambda$  defined as

$$\Lambda = \begin{bmatrix} S & 0 \\ 0 & S \end{bmatrix}, \quad (21)$$

the stabilized marching leapfrog scheme for Eq. (10),

$$\tilde{\theta}^{n+1} = S\tilde{u}^n, \quad \tilde{u}^{n+1} = S\tilde{\theta}^n + 2\Delta t S L \tilde{u}^n, \quad n = 1, 2, \dots, N, \quad (22)$$

may be written as

$$\tilde{V}^{n+1} = \Lambda G \tilde{V}^n, \quad n = 1, 2, \dots, N. \quad (23)$$

Note that with  $\tau^0$  as in Eq. (20),

$$\|V^1 - \tilde{V}^1\|_2 = \|\tau^0\|_2. \quad (24)$$

However, as will be seen later with data assimilation, it is possible for the true initial data  $u_0(x, y)$  in Eq. (19) to only be known approximately, leading to a significantly larger value for  $\|V^1 - \tilde{V}^1\|_2$ ,

$$\|V^1 - \tilde{V}^1\|_2 = A \gg \|\tau^0\|_2. \quad (25)$$

Unlike the case in Eq. (9), the linear difference scheme in Eq. (23) is susceptible to Fourier analysis. If  $L\tilde{u}^n \equiv h(x, y)$ , then its Fourier coefficients  $\{h_{j,k}\}$  are given by  $h_{j,k} = g_{j,k}\tilde{u}_{j,k}^n$ , where

$$g_{j,k} = -\{4\pi^2 a(j^2 + k^2) - 2\pi i(bj + ck)\}. \quad (26)$$

Hence, from Eqs. (6), (7) and (22),

$$\begin{aligned} \tilde{\theta}^{n+1} &= \sum_{j,k=-\infty}^{\infty} \sigma_{j,k} \tilde{u}_{j,k}^n \exp\{2\pi i(jx + ky)\}, \\ \tilde{u}^{n+1} &= \sum_{j,k=-\infty}^{\infty} \sigma_{j,k} \{\tilde{\theta}_{j,k}^n + 2\Delta t g_{j,k} \tilde{u}_{j,k}^n\} \exp\{2\pi i(jx + ky)\}. \end{aligned} \quad (27)$$

**Lemma 1** Let  $\lambda_{j,k}$ ,  $\sigma_{j,k}$ , be as in Eq. (6), let  $a$ ,  $b$ ,  $c$ , be as in Eq. (10), and let  $g_{j,k}$  be as in Eq. (26). Choose a positive integer  $J$  such that if  $\lambda_J = 4\pi^2 J$ , we have

$$\max_{(j^2+k^2) \leq J} \{|g_{j,k}|\} \leq 2a\lambda_J, \quad |g_{j,k}| \leq 2a\lambda_{j,k}, \quad \forall (j^2 + k^2) > J. \quad (28)$$

With  $p > 1$ , choose  $\omega \geq 4a(\lambda_J)^{1-p}$  in Eq. (6). Then,

$$\sigma_{j,k} (1 + 2|\Delta t||g_{j,k}|) \leq 1 + 4a|\Delta t|\lambda_J. \quad (29)$$

Hence,

$$\| \Lambda G \|_2 < 1 + 4a|\Delta t|\lambda_J < \exp\{4a|\Delta t|\lambda_J\}, \quad (30)$$

and, for  $n = 1, 2, \dots, N$ ,

$$\| \tilde{V}^{n+1} \|_2 = \| (\Lambda G)^n \tilde{V}^1 \|_2 < \exp\{4an|\Delta t|\lambda_J\} \| \tilde{V}^1 \|_2. \quad (31)$$

Therefore, with this choice of  $(\omega, p)$ , the linear leapfrog scheme in Eq. (23), is unconditionally stable, marching forward or backward in time.

*Proof:* We first show how to find a positive integer  $J$  such that Eq. (28) is valid. We have  $|g_{j,k}|^2 = a^2\lambda_{j,k}^2 + 4\pi^2(bj + ck)^2 \leq a^2\lambda_{j,k}^2 + 2d^2\lambda_{j,k}$ , where  $0 < d = \max(|b|, |c|)$ . Choose a positive integer  $J$  such that  $4\pi^2J > (2d^2/a^2)$ . Then,  $\forall (j, k)$ ,  $|g_{j,k}|^2 \leq a^2\lambda_{j,k}^2 + a^2\lambda_J\lambda_{j,k}$ , which implies Eq. (28). Next, the inequality in Eq. (29) is valid whenever  $(j^2 + k^2) \leq J$ , since  $\sigma_{j,k} \leq 1$ . For  $(j^2 + k^2) > J$ , we have  $\lambda_J < \lambda_{j,k}$  and  $|g_{j,k}| \leq 2a\lambda_{j,k}$ . Hence

$$\sigma_{j,k} = \exp\{-\omega|\Delta t|\lambda_{j,k}^p\} \leq \exp\{-\omega|\Delta t|\lambda_{j,k}\lambda_J^{p-1}\} \leq \exp\{-4a|\Delta t|\lambda_{j,k}\}, \quad (32)$$

since  $\omega\lambda_J^{p-1} \geq 4a$ . Also,  $\exp\{-4a|\Delta t|\lambda_{j,k}\} \leq (1 + 4a|\Delta t|\lambda_{j,k})^{-1}$ , since  $1 + x \leq e^x$  for real  $x$ . Hence, with  $|g_{j,k}| \leq 2a\lambda_{j,k}$  for  $(j^2 + k^2) > J$ , we find  $\sigma_{j,k}(1 + 2|\Delta t||g_{j,k}|) \leq 1$ . Thus, Eq. (29) is valid  $\forall (j, k)$ .

We now establish the stability inequality in Eq. (30). From Eq. (17) and Parseval's relation,

$$\| \tilde{V}^n \|_2^2 = \sum_{j,k=-\infty}^{\infty} (|\tilde{\theta}_{j,k}^n|^2 + |\tilde{u}_{j,k}^n|^2), \quad n = 1, 2, \dots, N+1. \quad (33)$$

From Eq. (27),

$$\tilde{\theta}_{j,k}^{n+1} = \sigma_{j,k}\tilde{u}_{j,k}^n, \quad \tilde{u}_{j,k}^{n+1} = \sigma_{j,k}\{\tilde{\theta}_{j,k}^n + 2\Delta t g_{j,k}\tilde{u}_{j,k}^n\}, \quad (34)$$

and

$$|\tilde{\theta}_{j,k}^{n+1}|^2 = \sigma_{j,k}^2 |\tilde{u}_{j,k}^n|^2, \quad (35)$$

$$|\tilde{u}_{j,k}^{n+1}|^2 \leq \sigma_{j,k}^2 |\tilde{\theta}_{j,k}^n|^2 + 4\Delta t^2 \sigma_{j,k}^2 |g_{j,k}|^2 |\tilde{u}_{j,k}^n|^2 + 4|\Delta t| \sigma_{j,k}^2 |g_{j,k}| |\tilde{\theta}_{j,k}^n \tilde{u}_{j,k}^n|.$$

Using  $2|\tilde{\theta}_{j,k}^n \tilde{u}_{j,k}^n| \leq |\tilde{\theta}_{j,k}^n|^2 + |\tilde{u}_{j,k}^n|^2$ , we have

$$4|\Delta t| \sigma_{j,k}^2 |g_{j,k}| |\tilde{\theta}_{j,k}^n \tilde{u}_{j,k}^n| \leq 2|\Delta t| \sigma_{j,k}^2 |g_{j,k}| |\tilde{\theta}_{j,k}^n|^2 + 2|\Delta t| \sigma_{j,k}^2 |g_{j,k}| |\tilde{u}_{j,k}^n|^2. \quad (36)$$

Hence, from Eqs. (35), (36),

$$|\tilde{\theta}_{j,k}^{n+1}|^2 + |\tilde{u}_{j,k}^{n+1}|^2 < (|\tilde{\theta}_{j,k}^n|^2 + |\tilde{u}_{j,k}^n|^2) \sigma_{j,k}^2 (1 + 2|\Delta t||g_{j,k}|)^2, \quad n = 1, 2, \dots, N. \quad (37)$$

Therefore, on using Eq. (29) in Eq. (37), together with Eq. (33),

$$\| \tilde{V}^{n+1} \|_2 = \| \Lambda G \tilde{V}^n \|_2 \leq (1 + 4a|\Delta t| \lambda_J) \| \tilde{V}^n \|_2, \quad (38)$$

and Eqs. (30) and (31), follow from Eqs. (38) and (17). QED.

With a change in notation, where the present  $u^n(x, y)$  is denoted by  $\omega^n(x, y)$ , and the present positive constant  $\omega$  in Eq. (6) is denoted by  $\gamma$ , the following result is stated and proved as Lemma 5.2 in Ref. [22].

**Lemma 2** *Let  $u^n(x, y) \equiv u(x, y, n\Delta t)$  be the exact solution in Eq. (10). Let  $\omega$ ,  $p$ ,  $\lambda_{j,k}$ ,  $\sigma_{j,k}$ , be as in Eq. (6). Let  $P$  and  $S$  be as in Eq. (7), let  $L$  be the linear operator in Eq. (10), and let  $\tau^n$  be as in Eq. (13). With the norm definition in Eq (18), and  $1 \leq n \leq N$ ,*

$$\begin{aligned} \| \tau^n \|_2 &\leq (1/6) |\Delta t|^3 \| |u_{ttt}| \|_{2,\infty}, \\ \| u^n - Su^n \|_2 &\leq \omega |\Delta t| \| |Pu| \|_{2,\infty}, \\ |\Delta t| \| Lu^n - SLu^n \|_2 &\leq \omega (\Delta t)^2 \| |PLu| \|_{2,\infty}. \end{aligned} \quad (39)$$

Moreover, with  $V^n$  as in Eq. (14),

$$\| GV^n - \Lambda GV^n \|_2 \leq \omega K \sqrt{3} |\Delta t| \| |Pu| \|_{2,\infty}, \quad (40)$$

where the constant  $K$  is given by

$$K = \{1 + (8/3)(\Delta t)^2 \| |PLu| \|_{2,\infty}^2 / \| |Pu| \|_{2,\infty}^2\}^{1/2}. \quad (41)$$

While the stabilized leapfrog scheme is unconditionally stable running forward or backward in time, it introduces a small error at each time step  $\Delta t$ , whose cumulative effect does not vanish as  $|\Delta t| \downarrow 0$ . Returning to Eq. (10), the well-posed forward problem, with  $\Delta t > 0$ , is considered first.

**Theorem 1** *With  $\Delta t > 0$  and  $T = (N + 1)\Delta t$ , let  $u^n(x, y)$  be the unique exact solution of Eq. (10) at  $t = n\Delta t$ , where  $a$ ,  $|b|$ ,  $|c| > 0$ . Let  $P$  and  $S$  be the operators defined in Eq. (7). With  $\lambda_J$  as in Lemma 1, let  $p > 1$ , and let  $\omega = 4a\lambda_J^{1-p}$  in the smoothing operator  $S$ . Let  $V^n$  be as in Eq. (14), let  $\tilde{V}^n$  be the solution of the forward leapfrog scheme in Eq. (23), and let  $K$  be the constant defined in Eq. (41). If  $E^n = V^n - \tilde{V}^n$  denotes the error at  $t_n = n\Delta t$ ,  $n = 1, 2, \dots, N + 1$ , we have, with the norm definitions in Eq. (18)*

$$\begin{aligned} \| E^n \|_2 &\leq \sqrt{3} K (\lambda_J)^{-p} \{ \exp(4a\lambda_J t_n) - 1 \} \| |Pu| \|_{2,\infty} \\ &\quad + (24a\lambda_J)^{-1} (\Delta t)^2 \{ \exp(4a\lambda_J t_n) - 1 \} \| |u_{ttt}| \|_{2,\infty} \\ &\quad + \exp(4a\lambda_J t_n) \| V^1 - \tilde{V}^1 \|_2. \end{aligned} \quad (42)$$

*Proof:* Let  $\Psi^n = \Phi_\tau^n + (GV^n - \Lambda GV^n)$ , where  $\Phi_\tau^n$  is as defined in Eq. (14). Then,  $E^{n+1} = \Lambda GE^n + \Psi^n$ , and

$$E^{n+1} = (\Lambda G)^n E^1 + \Delta t \sum_{j=0}^{n-1} (\Lambda G)^j \Psi^{n-j} / (\Delta t), \quad n = 1, 2, \dots, N. \quad (43)$$

**Table 1**

Values of constants  $C1 - C3$  in Eq. (46), with following parameter values:  
 $T = 1 \times 10^{-4}$ ,  $|\Delta t| = 5 \times 10^{-8}$ ,  $a = 1$ ,  $p = 3$ ,  $\omega = 2 \times 10^{-7}$ ,  $\lambda_J = 4472$ .

$C1 = e^{4aT\lambda_J}$	$C2 = (\lambda_J)^{-p}(C1 - 1)$	$C3 = \{(24a\lambda_J)^{-1}(\Delta t)^2(C1 - 1)\}$
$C1 < 5.99$	$C2 < 5.58 \times 10^{-11}$	$C3 < 1.17 \times 10^{-19}$

Hence

$$\begin{aligned} \|E^{n+1}\|_2 &\leq \|(\Lambda G)^n\| \|V^1 - \tilde{V}^1\|_2 \\ &\quad + \max_k \{\|\Psi^k\|_2 / \Delta t\} \Delta t \sum_{j=0}^{n-1} \|(\Lambda G)^j\|_2. \end{aligned} \quad (44)$$

From Eq. (31) in Lemma 1,  $\|(\Lambda G)^k\|_2 \leq \exp\{4a\lambda_J t_k\}$ . Also,

$$\Delta t \sum_{j=0}^{n-1} \|(\Lambda G)^j\|_2 \leq \int_0^{t_n} e^{4as\lambda_J} ds = \exp\{(4a\lambda_J t_n) - 1\} / (4a\lambda_J). \quad (45)$$

From Eq. (39) in Lemma 2,  $\|\Phi_\tau^n\|_2 \leq (1/6)|\Delta t|^3 \|u_{ttt}\|_{2,\infty}$ , while  $\|GV^n - \Lambda V^n\|_2$  satisfies Eq. (40) in Lemma 2, with  $\omega = 4a(\lambda_J)^{1-p}$ . Therefore, Eq. (42) follows after applying Eq. (45) in Eq. (44). QED.

**Remark 1.** The first term on the right hand side in Eq. (42) is the *stabilization penalty*, which is the price that must be paid for using the leapfrog scheme in the computation of the well-posed forward linear problem in Eq. (10). Without stabilization, the leapfrog scheme is unconditionally unstable for that forward problem, and no error bound is possible. If the initial data  $u_0(x, y)$  in Eq. (19) are known exactly, then, from Eq. (24),  $\|V^1 - \tilde{V}^1\|_2 = \|\tau^0\|_2$ , and the last term on the right in Eq. (42) is  $O(\Delta t)^2$ . However, as may be seen from Eq. (47) and Table 1 below, with appropriate parameter values, useful results may still be possible if the initial data in Eq. (19) merely approximate the true values.

Define the constants  $C1$ ,  $C2$ ,  $C3$ ,  $C4$ , as follows

$$\begin{aligned} C1 &= e^{4aT\lambda_J}, \quad C2 = \{(\lambda_J)^{-p}(C1 - 1)\}, \quad C3 = \{(24a\lambda_J)^{-1}(\Delta t)^2(C1 - 1)\}, \\ C4 &= \sqrt{3}K C2 \|Pu\|_{2,\infty} + C3 \|u_{ttt}\|_{2,\infty}. \end{aligned} \quad (46)$$

Using Eq. (42), we have

$$\max_n \|E^n\|_2 \leq C1 \|V^1 - \tilde{V}^1\|_2 + C4. \quad (47)$$

In the ill-posed backward problem, we contemplate marching backward in time from  $t = T = (N + 1)|\Delta t|$ , using negative time steps  $\Delta t$ . However, the needed initial data

$u_0(x, y) \equiv u(x, y, T)$ , where  $u(x, y, t)$  is the unique exact solution in Eq. (10), are seldom known exactly. For this reason, the ill-posed backward problem is generally formulated as follows:

With  $\Delta t < 0$ , target data  $g(x, y)$  are given and assumed to approximate true data  $u(x, y, T)$ , while  $g + \Delta t Lg$  approximates true data  $u(x, y, T - |\Delta t|)$ , both in the  $\mathcal{L}^2(\Omega)$  norm. Moreover, the unique true backward solution  $u(x, y, t)$  corresponding to the unknown exact data  $u(x, y, T)$ , is such that both  $u(x, y, 0)$  and  $u(x, y, |\Delta t|)$  satisfy known  $\mathcal{L}^2(\Omega)$  bounds. Specifically, for some  $\delta > 0$ , *presumed* known and small, and some  $M \gg \delta$ ,

$$\begin{aligned} \|g - u(\cdot, T)\|_2^2 + \|(g + \Delta t Lg) - u(\cdot, T - |\Delta t|)\|_2^2 &\leq \delta^2, \\ \|u(\cdot, 0)\|_2^2 + \|u(\cdot, |\Delta t|)\|_2^2 &\leq M^2. \end{aligned} \quad (48)$$

Analogously to the well-posed forward problem in Eq. (23), we now choose  $\Delta t < 0$  and consider the stabilized leapfrog scheme marching backward from  $t = T$  with the given data  $g(x, y)$  in Eq. (48)

$$\tilde{V}^{n+1} = \Lambda G \tilde{V}^n, \quad n = 1, 2, \dots, N, \quad \tilde{V}^1 = [g, (g + \Delta t Lg)]^T, \quad (49)$$

where, with  $\delta$ ,  $M$  as in Eq. (48),  $\Phi_\tau^n$  as in Eq. (14), and  $n = 1, 2, \dots, N$ , the true solution satisfies

$$V^{n+1} = G V^n + \Phi_\tau^n, \quad \|V^1 - \tilde{V}^1\|_2 \leq \delta, \quad \|V^{N+1}\|_2 \leq M. \quad (50)$$

Proof of the next result follows the same steps used in the preceding Theorem.

**Theorem 2** *With  $g(x, y)$ ,  $M$ ,  $\delta$ , as in Eq. (48),  $\Delta t < 0$ , and  $T = (N + 1)|\Delta t|$ , let  $V^n$  be the exact solution of the backward problem in Eq. (50) at time  $T - n|\Delta t|$ ,  $n = 1, 2, \dots, N + 1$ . With  $a$ ,  $p$ ,  $\lambda_J$ , as in Lemma 1, let  $\omega = 4a(\lambda_J)^{1-p}$  in the smoothing operator  $S$  in Eq. (7). Let  $\tilde{V}^n$  be the corresponding solution of the stabilized backward leapfrog scheme in Eq. (49), let  $K$  be the constant in Eq. (41), and let  $E^n \equiv V^n - \tilde{V}^n$  denote the error at time  $T - n|\Delta t|$ . Then, for  $n = 1, 2, \dots, N + 1$  with the norm definitions in Eq. (18)*

$$\begin{aligned} \|E^n\|_2 &\leq \sqrt{3} K (\lambda_J)^{-p} \{\exp(4an|\Delta t|\lambda_J) - 1\} \|Pu\|_{2,\infty} \\ &\quad + (24a\lambda_J)^{-1} (\Delta t)^2 \{\exp(4an|\Delta t|\lambda_J) - 1\} \|u_{ttt}\|_{2,\infty} \\ &\quad + \delta \exp\{4an|\Delta t|\lambda_J\}. \end{aligned} \quad (51)$$

Using Eq. (51), and the definitions in Eq. (46), we have

$$\max_n \|E^n\|_2 \leq C1 \delta + C4. \quad (52)$$

**Remark 2** The stability analysis of the linear constant coefficient problem presented in this section, provides valuable insight into the difficulties attending data assimilation in

dissipative evolution equations. In that context,  $g(x, y)$  in the above Theorem represents possibly non smooth target data  $u^*(x, y, T)$ , differing from an actual solution  $u(x, y, T)$  by an unknown amount  $\delta$  in the  $\mathcal{L}^2(\Omega)$  norm. Marching backward from  $T > 0$  with  $g(x, y)$ , leads to the error  $E^{N+1}$  at  $t = 0$ , obeying Eq. (52) with the definitions in Eq. (46). The computed backward solution at  $t = 0$  is now used as the initial data  $\tilde{V}^1$  in the forward computation discussed in the preceding Theorem. However,  $\tilde{V}^1$  is only an approximation to the true initial data  $V^1$ , with  $\|V^1 - \tilde{V}^1\|_2 \leq C1 \delta + C4$ , from Eq. (52). Hence, from Eq. (47), the forward computation with such approximate initial data leads to an error  $E^{N+1}$  at time  $T > 0$  satisfying

$$\|E^{N+1}\|_2 \leq C1 (C1 \delta + C4) + C4 = (C1)^2 \delta + C4(C1 + 1) \quad (53)$$

The feasibility of data assimilation hinges on the true value of  $\delta > 0$ , together with the values for  $\|Pu\|_{2,\infty}$ ,  $\|u_{ttt}\|_{2,\infty}$ ,  $T$ ,  $|\Delta t|$ ,  $a$ ,  $p$ ,  $\omega$ , and  $\lambda_J = (\omega/4a)^{1/(1-p)}$ . With the parameter values listed in Table 1, Eq. (53) gives  $\|E^{N+1}\|_2 < 36 \delta + 7 C4$ , where  $C4$  may be expected to be negligibly small, given the values for  $C2$ ,  $C3$ . This leads to successful assimilation, provided  $\delta$  is reasonably small. However, if in Table 1 we choose  $T$  three times larger, and  $\omega$  ten times smaller, we find  $\lambda_J = 14142$ ,  $C1 = 2.35 \times 10^7$ ,  $C2 = 8.29 \times 10^{-6}$ ,  $C3 = 1.73 \times 10^{-13}$ . With  $(C1)^2 = 5.53 \times 10^{14}$ , useful data assimilation is unlikely.

## 5. Leapfrog Nonlinear Computational Instability and the RAW Filter

The results in Theorems 1 and 2 indicate that the stabilizing approach in Eqs. (23) and (49), is sound for the leapfrog scheme applied to the linearized problem, and that it can deliver useful results at realistic parameter values. In the case of the  $O(\Delta t)$  pure explicit scheme discussed in Ref. [12], such linear stability analysis was found to carry over to the nonlinear problem. However, as has been known for some time, for the  $O(\Delta t)^2$  leapfrog scheme, linear stability is necessary but not sufficient in the presence of nonlinearities.

In recent years, effective methods of preventing leapfrog nonlinear instability have been developed and analyzed [25–27]. These are post processing time domain filtering techniques, which are applied at every time step, and which consist of replacing the computed solution with a specific linear combination of computations at previous time steps. Such techniques can also be usefully applied in the present 2D nonlinear advection diffusion problem.

We first describe the Robert-Asselin-Williams filter (RAW) [26, 27] as it applies to the stabilized leapfrog scheme for the forward nonlinear problem with the nonlinear operator  $L^\dagger$  previously defined in Eq. (8), together with the smoothing operator  $S$  defined in Eq. (7). With  $\Delta t > 0$ , and with  $\tilde{u}^n(x, y) \equiv \tilde{u}(x, y, n\Delta t)$ , denoting the intended approximation to  $u(x, y, n\Delta t)$ , let

$$\tilde{\theta}^1(x, y) = u_0(x, y), \quad \tilde{u}^1(x, y) = u_0(x, y) + \Delta t L^\dagger \tilde{\theta}^1. \quad (54)$$

This forward problem is defined by

$$\begin{aligned}\tilde{\theta}^{n+1} &= S\tilde{u}^n, \\ \tilde{u}^{n+1} &= S\tilde{\theta}^n + 2\Delta t SL^\dagger \tilde{u}^n, \quad n = 1, 2, \dots, N.\end{aligned}\tag{55}$$

For  $n = 1, 2, \dots, N$ , the forward problem is modified as follows under RAW filtering. With positive constants  $\xi$ ,  $\eta$ , where  $\xi = 0.53$ , and  $0.01 \leq \eta \leq 0.2$ , and with  $\overline{\tilde{u}}^1 = \tilde{u}^1$ ,  $\overline{\tilde{\theta}}^1 = \tilde{\theta}^1$ ,

$$\begin{aligned}\tilde{\theta}^{n+1} &= S\overline{\tilde{u}}^n, \\ \tilde{u}^{n+1} &= S\overline{\tilde{\theta}}^n + 2\Delta t SL^\dagger \overline{\tilde{u}}^n, \\ \overline{\tilde{\theta}}^{n+1} &= \tilde{\theta}^{n+1} + 0.5\xi\eta \left( \tilde{u}^{n+1} - 2\tilde{\theta}^{n+1} + \tilde{\theta}^n \right), \\ \overline{\tilde{u}}^{n+1} &= \tilde{u}^{n+1} - 0.5\eta(1 - \xi) \left( \tilde{u}^{n+1} - 2\overline{\tilde{\theta}}^{n+1} + \tilde{\theta}^n \right),\end{aligned}\tag{56}$$

with the filtered arrays  $\overline{\tilde{\theta}}^{n+1}$ ,  $\overline{\tilde{u}}^{n+1}$ , overwriting the unfiltered arrays  $\tilde{\theta}^{n+1}$ ,  $\tilde{u}^{n+1}$ , at each time step. With given data  $g(x, y)$  for  $\tilde{u}(x, y, T)$  satisfying Eq. (48), and  $\tilde{\theta}^1 = g(x, y)$ ,  $\tilde{u}^1 = g + \Delta t L^\dagger g$ , with  $\Delta t < 0$ , the backward problem is modified in exactly the same way. The recommended value  $\xi = 0.53$  in Ref. [26] is designed to maintain the  $O(\Delta t)^2$  accuracy in the leapfrog scheme.

**Remark 3.** Prior information about the solution is essential in ill-posed inverse problems. When data assimilation is feasible, interactive adjustment of the pair  $(\omega, p)$  in Eqs. (6, 7) in the smoothing operator  $S$ , often leads to useful results. This process is similar to the manual tuning of an FM station, or the manual focusing of binoculars, and likewise requires user recognition of a correct solution. Beginning with small values of  $\omega$  and  $p$ , chosen so as not to oversmooth the solution, a small number of successive trials are performed. Because of the underlying *explicit* marching difference scheme, this can be accomplished in a relatively short time. The values of  $(\omega, p)$  are increased slowly if instability is detected, and are likewise decreased slowly to increase sharpness, provided no instability results. As is the case with binoculars, when data assimilation is feasible, useful results are obtained after relatively few trials. There may be several possible good solutions.

## 6. 2D Nonlinear Computational Experiments

It remains to be seen whether the simplified linear analysis in Section 4 is predictive of behavior in the following nonlinear advection diffusion equation in the unit square  $\Omega \subset \mathbb{R}^2$ ,

$$u_t = \alpha(u)\nabla \cdot \{q(x, y)\nabla u\} + \beta(u)u_x + \gamma(u)u_y.\tag{57}$$

where

$$\begin{aligned}\alpha(u) &= \exp(0.0165u), & q(x,y) &= 0.001(1.0 + 2(\sin(\pi x))(\exp(2y))), \\ \beta(u) &= 0.417u\exp(2\cos(u)), & \gamma(u) &= 4u.\end{aligned}\tag{58}$$

In the following 5 numerical experiments, a  $512 \times 512$  equispaced grid is placed on the unit square  $\Omega$ . Second order accurate centered finite differencing is used for the space variables in the fully discrete nonlinear leapfrog scheme corresponding to Eq. (9). With  $|\Delta t| = 5.0 \times 10^{-8}$ ,  $\omega = 2.0 \times 10^{-7}$ , and  $p = 3.0$ , Fast Fourier Transform (FFT) algorithms are used to synthesize the smoothing operator  $S$  defined in Eq. (7), and RAW filtering is applied at every time step in accordance with Eq. (56).

With  $\overline{u}^{N+1}(x,y)$  in Eq. (56) the computed approximation to the given target data  $u^*(x,y,T)$  at  $T = (N+1)|\Delta t|$ , we compute the  $\mathcal{L}^1(\Omega)$  relative errors,  $\|\overline{u}^{N+1} - u^*(., T)\|_1 / \|u^*(., T)\|_1$ , and the  $\mathcal{L}^2(\Omega)$  peak signal to noise ratios  $PSNR$ , where

$$PSNR = 20.0 \log_{10} \left\{ 255.0 (\|\overline{u}^{N+1} - u^*(., T)\|_2)^{-1} \right\}.\tag{59}$$

Highly successful data assimilation would require an  $\mathcal{L}^1$  relative error on the order of 10% or less, with a  $PSNR \geq 30$ .

In all five experiments, the target data  $u^*(x,y,T)$  are given at  $T = 1.0 \times 10^{-4}$ . Significantly better results are obtained with  $T$  chosen ten times smaller. However, the aim in the present paper is to illustrate data assimilation behavior given a  $T$  value that is presumed adequate. In the Bill Clinton image in Fig. 2, the target data in the leftmost column are run backward to time  $t = 0$ , to produce the candidate initial data in the middle column. These data are now marched forward in time, to obtain the assimilated data in the rightmost column. Here, an  $\mathcal{L}^1$  relative error of 18% with  $PSNR = 19$  in Table 2, together with the image and contour plot in the rightmost column, indicate modestly successful assimilation.

Better results are achieved with the Hubble telescope barred spiral galaxy image in Fig. 3. In Table 3, we find an  $\mathcal{L}^1$  relative error of 16% with  $PSNR = 27$ . The image and contour plot in the rightmost column are a fair approximation to the target data in the leftmost column.

Significantly less success is achieved in the jet engine image in Fig. 4. In Table 4, we find an  $\mathcal{L}^1$  relative error of 33% with  $PSNR = 16$ . The contour plot in the rightmost column is an unsatisfactory approximation to the corresponding plot in the leftmost column.

The next two experiments involve the 1951 USAF resolution chart image. These two experiments are aimed at the practical situation where, although the target data and  $T$  value are given accurately, the actual values of the nonlinear coefficients  $\alpha(u)$ ,  $\beta(u)$ ,  $\gamma(u)$ , in Eq. (58) are only tentatively known or surmised, and may need readjustment.

Significant failure is evident in Fig. 5, using the original nonlinearities in Eq. (58). In Table 5, we find an  $\mathcal{L}^1$  relative error of 102% with  $PSNR = 11$ . In neither the image nor the contour plot, can the small characters be identified in the rightmost column data.

However, the direct, accurate, and relatively fast leapfrog computations described in Eq. (56), allow for easy experimentation with successively smaller nonlinearities. With new coefficients 6 times smaller,  $\alpha(u) = \exp(0.00275u)$ ,  $\beta(u) = 0.0695u \exp(2\cos(u))$ ,  $\gamma(u) = 0.667u$ , there is noticeable improvement and modestly successful assimilation in Fig. 6, with an  $\mathcal{L}^1$  relative error of 48% with  $PSNR = 15$ . Clearly, many other choices for  $\alpha(u)$ ,  $\beta(u)$ ,  $\gamma(u)$ , may be found that would result in equally successful assimilation. The experiment in Fig. 6 merely indicates a need for reconsideration of the physics that led to Eq. (58).

## 7. Concluding Remarks

A stable, second order accurate, backward marching explicit finite difference scheme, was applied to explore difficulties that inevitably arise in data assimilation in nonlinear advection diffusion equations. These difficulties originate from ill-posedness of the inverse problem, together with non smooth target data that may not correspond to an actual solution of the evolution equation at the prescribed time  $T > 0$ . Moreover, the value of  $T > 0$  at which target data are prescribed, must be small enough to be compatible with the governing nonlinearities. Instructive successful and unsuccessful examples were presented illustrating several key points.

The leapfrog scheme approach may be helpful in conjunction with more elaborate computationally intensive data assimilation procedures, by providing a preliminary assessment of the feasibility of the desired target data at a given  $T$  value, as well as possibly useful initial results. The scheme may also be used for prior experimentation with other  $T$  values, or with readjusted coefficients in the evolution equation.

## DATA ASSIMILATION IN BILL CLINTON IMAGE AT $T=1.0E-4$

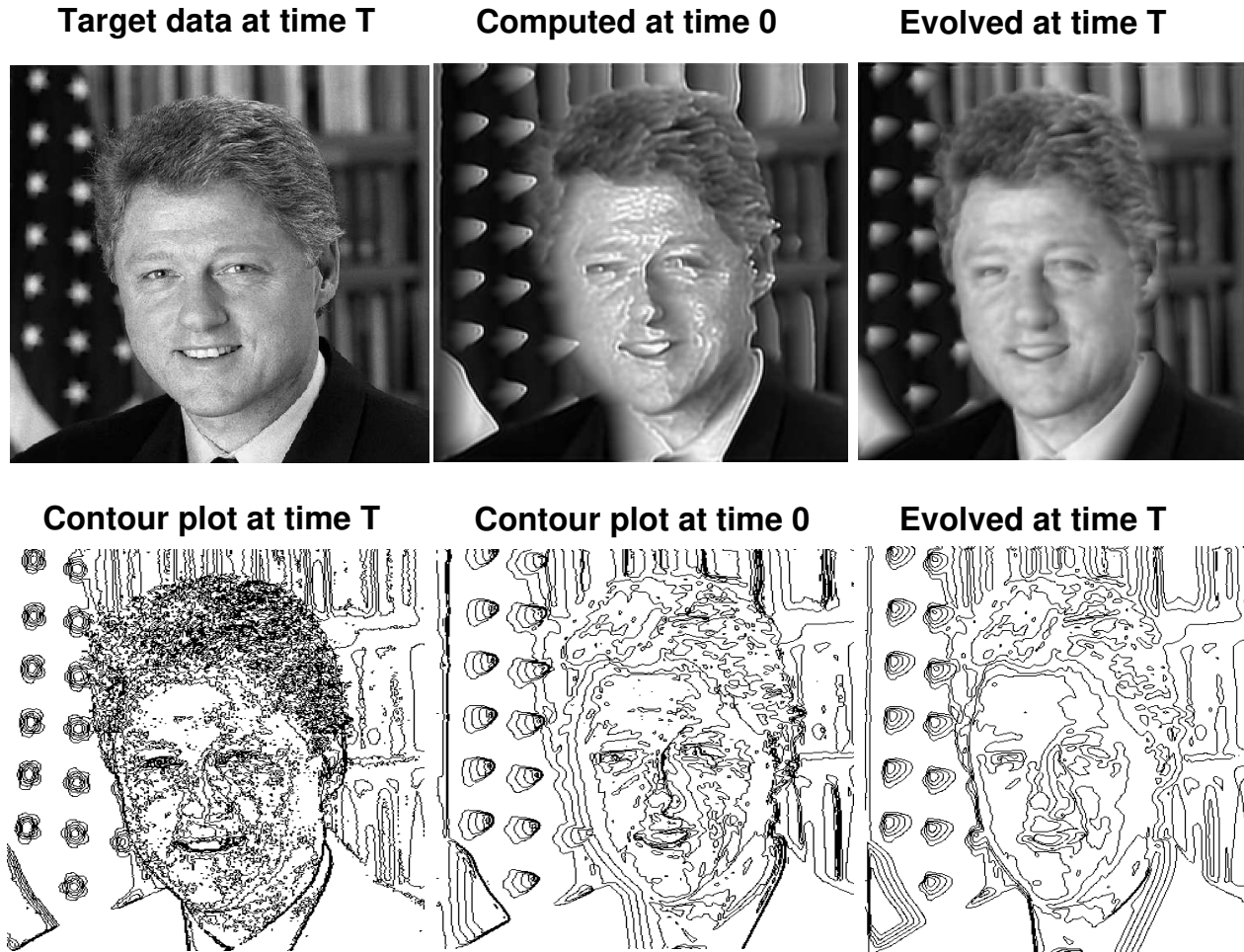


**Fig. 2.** Target data at time  $T$ , in leftmost column, are marched backward in time to obtain candidate initial data in middle column. When marched forward to time  $T$ , middle column data evolve into rightmost column. Quantitative error estimates are provided in Table 2.

**Table 2**

*President Clinton target image at  $T = 1.0 \times 10^{-4}$ .  
 $\mathcal{L}^1$ -norm behavior in data assimilation.*

<i>Target <math>\mathcal{L}^1</math> norm at <math>T</math></i>	<i>Computed at 0</i>	<i>Achieved at <math>T</math></i>	<i><math>\mathcal{L}^1</math> Rel Err</i>	<i>PSNR</i>
87.64	90.31	88.29	18.29 %	19.49

## DATA ASSIMILATION IN GALAXY IMAGE AT $T=1.0E-4$

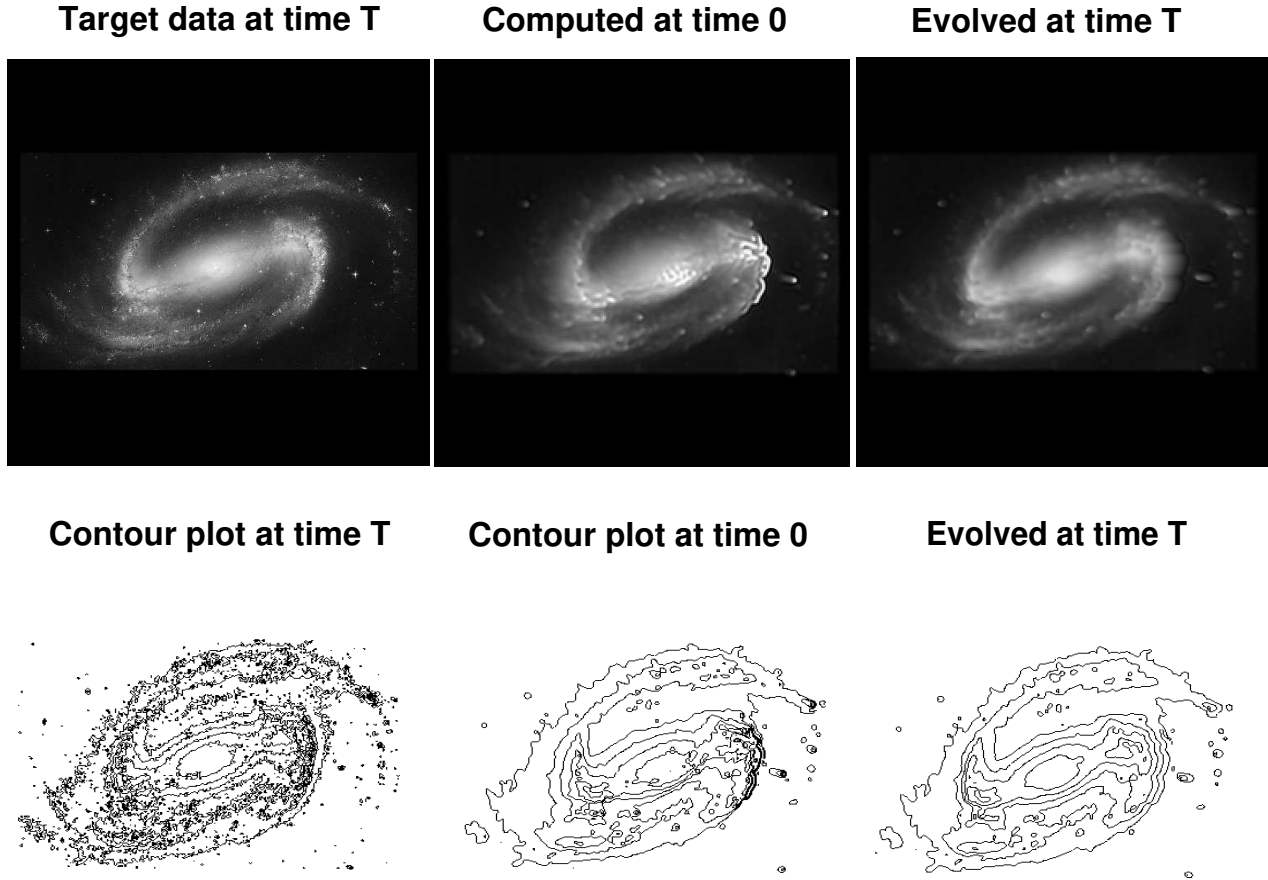


**Fig. 3.** Target data at time  $T$ , in leftmost column, are marched backward in time to obtain candidate initial data in middle column. When marched forward to time  $T$ , middle column data evolve into rightmost column. Quantitative error estimates are provided in Table 3.

**Table 3**

*Hubble telescope barred galaxy NGC1300 target image at  $T = 1.0 \times 10^{-4}$ .  
 $\mathcal{L}^1$ -norm behavior in data assimilation.*

<i>Target <math>\mathcal{L}^1</math> norm at <math>T</math></i>	<i>Computed at 0</i>	<i>Achieved at <math>T</math></i>	<i><math>\mathcal{L}^1</math> Rel Err</i>	<i>PSNR</i>
26.72	27.08	26.87	16.19 %	27.43

## DATA ASSIMILATION IN JET ENGINE IMAGE AT $T=1.0E-4$

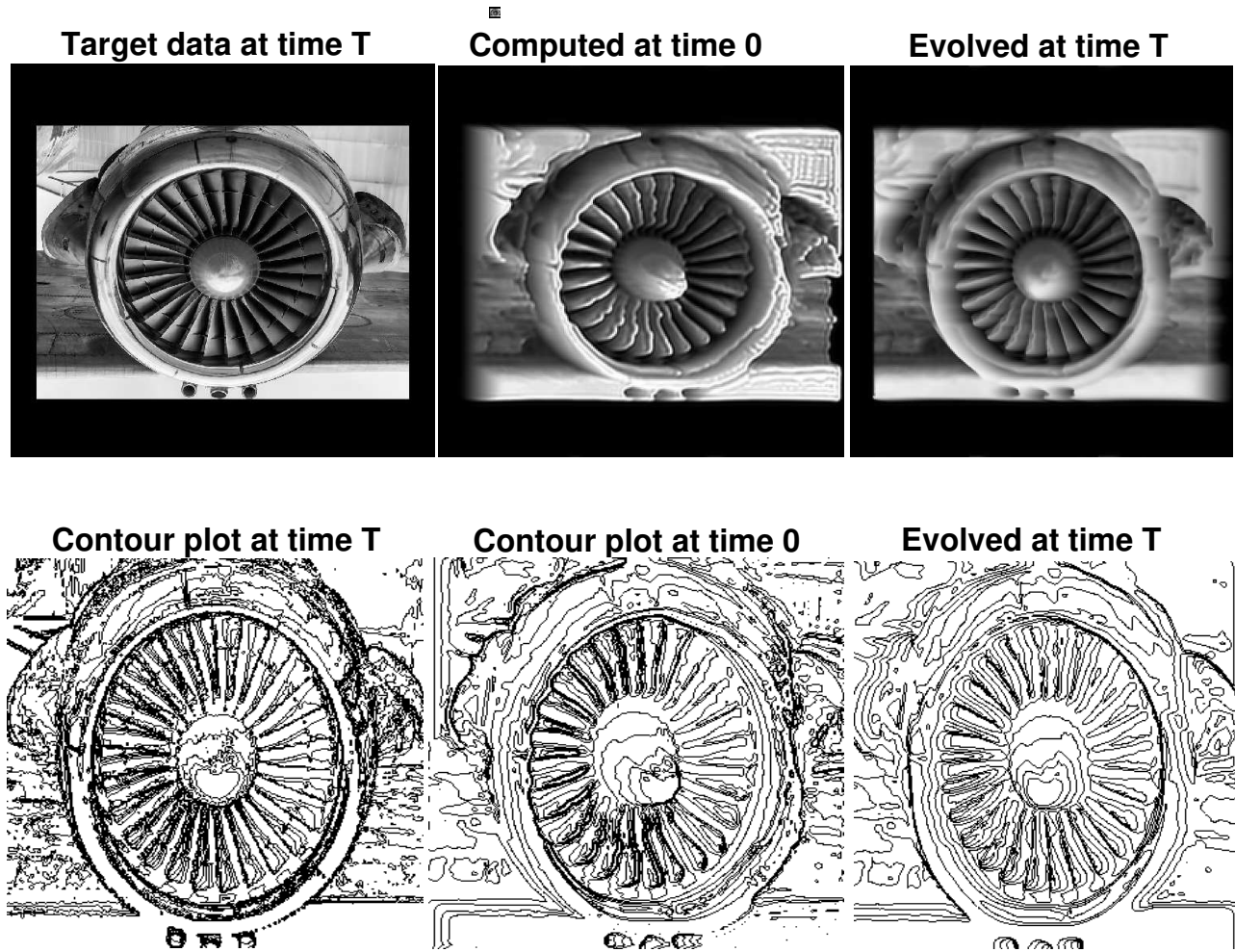


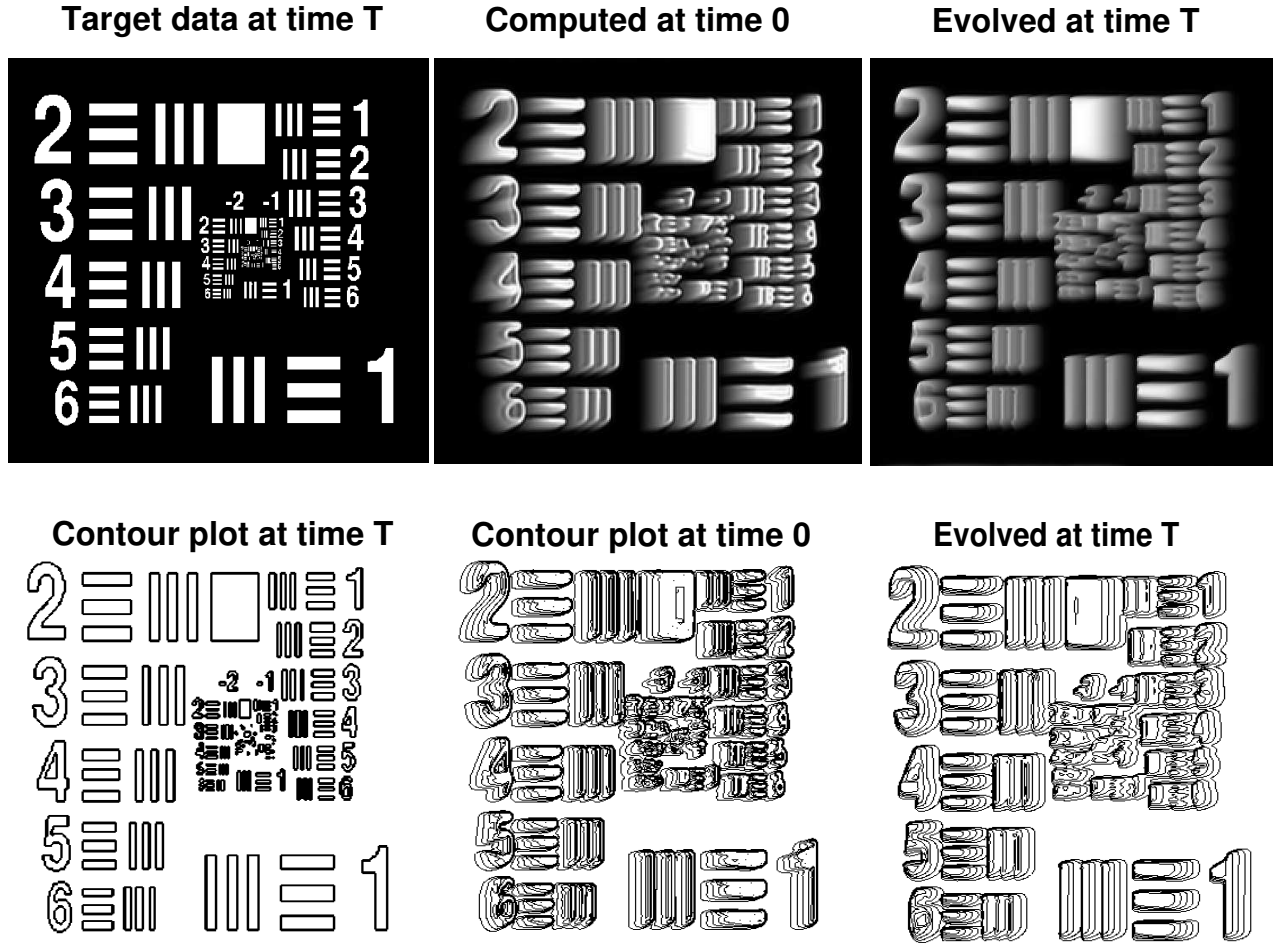
Fig. 4. Target data at time  $T$ , in leftmost column, are marched backward in time to obtain candidate initial data in middle column. When marched forward to time  $T$ , middle column data evolve into rightmost column. Quantitative error estimates are provided in Table 4.

Table 4

*Jet engine target image at  $T = 1.0 \times 10^{-4}$ .  
 $\mathcal{L}^1$ -norm behavior in data assimilation.*

<i>Target <math>\mathcal{L}^1</math> norm at <math>T</math></i>	<i>Computed at 0</i>	<i>Achieved at <math>T</math></i>	<i><math>\mathcal{L}^1</math> Rel Err</i>	<i>PSNR</i>
69.52	75.09	72.22	32.80 %	15.90

## DATA ASSIMILATION IN USAF CHART IMAGE AT $T=1.0E-4$



**Fig. 5.** Target data at time  $T$ , in leftmost column, are marched backward in time to obtain candidate initial data in middle column. When marched forward to time  $T$ , middle column data evolve into rightmost column. Quantitative error estimates are provided in Table 5.

**Table 5**

*USAF resolution chart target image at  $T = 1.0 \times 10^{-4}$ .  
 $\mathcal{L}^1$ -norm behavior in data assimilation.*

<i>Target <math>\mathcal{L}^1</math> norm at <math>T</math></i>	<i>Computed at 0</i>	<i>Achieved at <math>T</math></i>	<i><math>\mathcal{L}^1</math> Rel Err</i>	<i>PSNR</i>
46.75	57.41	52.93	102.28%	10.59

## DATA ASSIMILATION IN USAF CHART IMAGE AT $T=1.0E-4$ (after reducing nonlinearities in evolution equation)

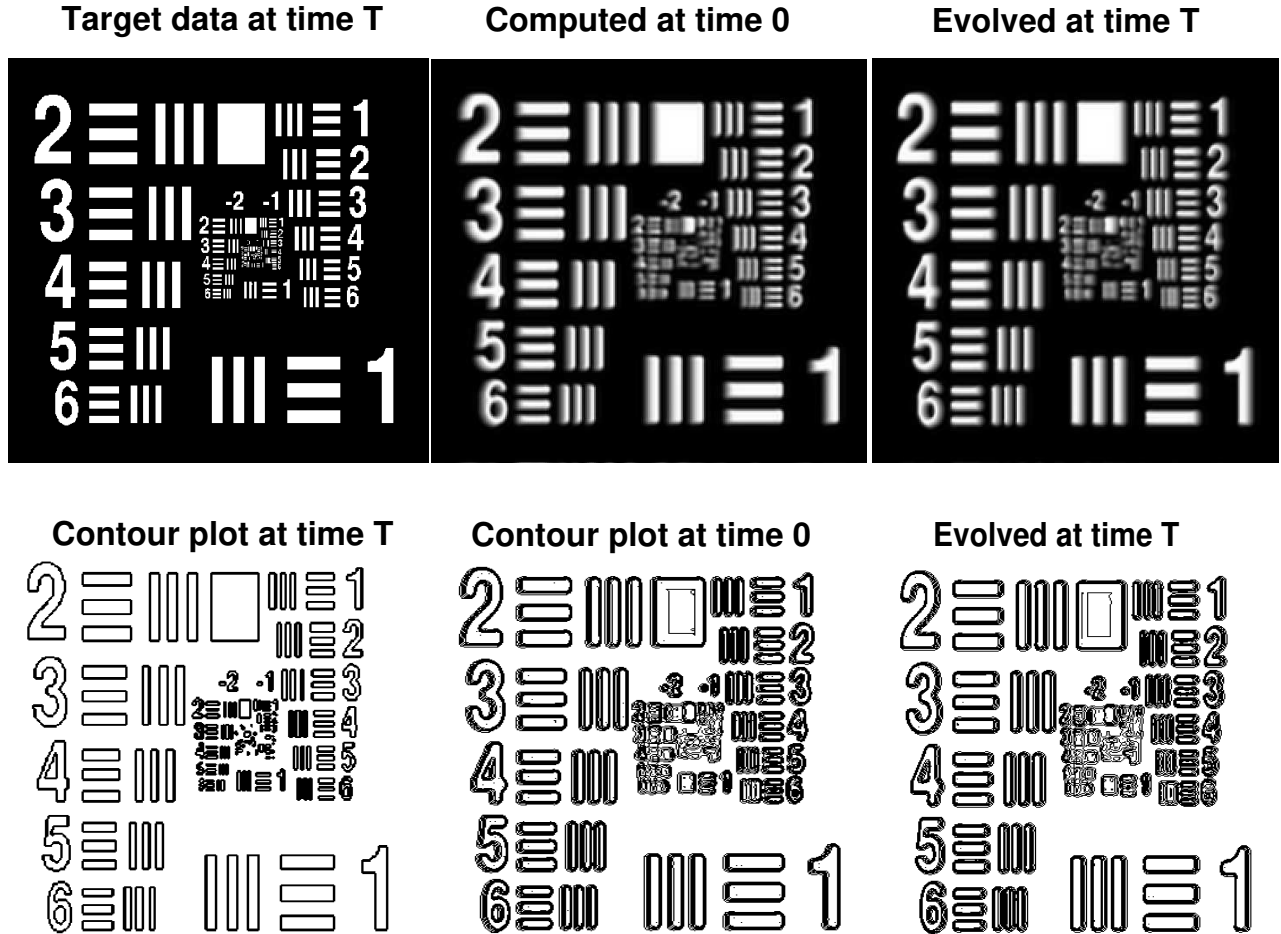


**Fig. 6.** Target data at time  $T$ , in leftmost column, are marched backward in time to obtain candidate initial data in middle column. When marched forward to time  $T$ , middle column data evolve into rightmost column. Quantitative error estimates are provided in Table 6.

**Table 6**

*USAF resolution chart target image at  $T = 1.0 \times 10^{-4}$ .  
 (after interactive reduction of nonlinearities in evolution equation.)  
 $\mathcal{L}^1$ -norm behavior in data assimilation.*

<i>Target <math>\mathcal{L}^1</math> norm at <math>T</math></i>	<i>Computed at 0</i>	<i>Achieved at <math>T</math></i>	<i><math>\mathcal{L}^1</math> Rel Err</i>	<i>PSNR</i>
46.75	48.56	48.27	48.08 %	15.15

## References

- [1] Singh R (2013) Advection diffusion equation models in near-surface geophysical and environmental sciences. *J Ind Geophys Union* 17(2):117–127.
- [2] Atmadja J, Bagtzoglou A (2001) State of the art report on mathematical methods for groundwater pollution source identification. *Environmental Forensics* 2:205–214.
- [3] Atmadja J, Bagtzoglou A (2001) Pollution source identification in heterogeneous porous media. *Water Resources Research* 37:2113–2125.
- [4] Gomez-Hernandez J, Xu T (2022) Contaminant source identification in aquifers: a critical view. *Math Geosci* 54:437–458.
- [5] He Q, Barajas-Solano D, Tartakovsky G (2020) Physics-informed neural networks for multiphysics data assimilation with application to subsurface transport. *Advances in Water Resources* <https://doi.org/10.1016/j.advwatres.2020.103610>
- [6] Arcucci R, Zhu J, Hu S (2021) Deep data assimilation: integrating deep learning with data assimilation. *Appl Sci* 11(1114). <https://doi.org/10.3390/app11031114>
- [7] Xu T, Zhang W, Gomez-Hernandez J (2022) Non-point contaminant source identification in an aquifer using the ensemble smoother with multiple data assimilation. *Journal of Hydrology* 606(127405).
- [8] Vukicevic T, Steyskal M, Hecht M (2001) Properties of advection algorithms in the context of variational data assimilation. *Monthly Weather Review* 129:1221–1231.
- [9] Ismail-Zadeh A, Korotkii A, Schubert G (2007) Quasi-reversibility method for data assimilation in models of mantle dynamics. *Geophys J Int* 170:1381–1398.
- [10] de Campos Velho HF, Barbosa VC, Cocke S (2013) Special issue on inverse problems in geosciences. *Inverse Problems in Science and Engineering* 21(3):355–356. <https://doi.org/10.1080/17415977.2012.712532>
- [11] Auroux D, Nodet M (2012) The back and forth nudging algorithm for data assimilation problems: theoretical results on transport equations. *ESAIM: COCV* 18:318–342.
- [12] Carasso A (2021) Data assimilation in 2D viscous Burgers equation using a stabilized explicit finite difference scheme run backward in time. *Inverse Probl Sci Eng* <https://doi.org/10.1080/17415977.2021.2009476>
- [13] Ames K, Straughan B (1997) *Non-Standard and Improperly Posed Problems*. Vol. 194 (Academic Press, New York).
- [14] Knops R (1973) Logarithmic convexity and other techniques applied to problems in continuum mechanics. *Symposium on non-well-posed problems and logarithmic convexity*, ed Knops R (Springer-Verlag, New York), *Lecture notes in mathematics*, Vol. 316.
- [15] Knops R, Payne L (1968) On the stability of solutions of the Navier-Stokes equations backward in time. *Arch Rat Mech Anal* 29:331–335.
- [16] Payne L (1971) Uniqueness and continuous dependence criteria for the Navier-Stokes equations. *Rocky Mountain J Math* 2:641–660.
- [17] Payne L (1992) Some remarks on ill-posed problems for viscous fluids. *Int J Engng Sci* 30:1341–1347.

- [18] Carasso A (2012) Reconstructing the past from imprecise knowledge of the present: Effective non-uniqueness in solving parabolic equations backward in time. *Math Methods Appl Sci* 36(249).
- [19] Carasso A (1977) Computing small solutions of Burgers' equation backwards in time. *J Math Anal App* 59:169–209.
- [20] Hào D, Nguyen V, Nguyen V (2015) Stability estimates for Burgers-type equations backward in time. *J Inverse Ill Posed Probl* 23:41–49.
- [21] Carasso A (2017) Stabilized Richardson leapfrog scheme in explicit stepwise computation of forward or backward nonlinear parabolic equations. *Inverse Probl Sci Eng* 25:1–24.
- [22] Carasso A (2021) Stabilized leapfrog scheme run backward in time, and the explicit  $O(\Delta t)^2$  stepwise computation of ill-posed time-reversed 2D Navier-Stokes equations. *Inverse Probl Sci Eng* <https://doi.org/10.1080/17415977.2021.1972997>
- [23] Carasso AS, Vladár AE (2008) Calibrating image roughness by estimating Lipschitz exponents, with applications to image restoration. *Optical Engineering* 47(3):1–13. <https://doi.org/10.1117/1.2899144>
- [24] Richtmyer R, Morton K (1967) *Difference Methods for Initial Value Problems* (Wiley, New York (NY), 2nd Ed.
- [25] Asselin R (1972) Frequency filter for time integrations. *Monthly Weather Review* 100:487–490.
- [26] Williams P (2009) A proposed modification to the robert-asselin time filter. *Monthly Weather Review* 137:2538–2546.
- [27] Williams P (2011) The rawfilter: An improvement to the robert-asselin filter in semi-implicit integrations. *Monthly Weather Review* 139:1996–2007.